DOI: 10.31276/VJSTE.65(4).36-41

Methyl orange-doped thiourea barium chloride crystals: Natural bond orbital analysis of the fock matrix for laser applications

S. Panimalar[1], P. Kumaresan[1], S. Nithiyanantham[2*], K. Selva Sambath Kumar[3], R. Mohan[4]

[1]PG & Research Department of Physics, Thiru A. Govindasamy Government Arts College, Tindivanam - 604 307, Tamil Nadu, India
[2]PG & Research Department of Physics, Thiru Vi. Ka. Govt. Arts College, Thiruvarur, Tamilnadu - 610 003, India
[3]PG & Research Department of Physics, Arignar Anna Government Arts College, Villupuram - 605 603, Tamil Nadu, India
[4]Department of Chemistry, Presidency University, Bangalore -560 064, India

Received 8 April 2023; revised 9 May 2023; accepted 5 July 2023

Abstract:

Pure thiourea barium chloride (TBC) crystals were synthesised using a slow cooling rate (0.05°C/day) and gradual evaporation from an aqueous solution. The growth process occurred over more than 19 days at a temperature of 39°C. Natural bond orbital (NBO) analysis has proven beneficial for studying charge transfer and conjugative interactions in molecular systems. Moreover, it sheds light on intermolecular bonding, and the interactions between these bonds have implications for optical applications. Additionally, the charge transfer interactions within the molecule that influence its catalytic activity can be elucidated by a lower HOMO and LUMO energy gap. This energy difference can be an indicator of a compound's excitability; the more readily a compound can be excited, the narrower the energy gap. The energy gap might be significantly affected by the influence of thermal energy. The non-linear optical (NLO) efficiency of methyl orange-doped (MOD) TBC crystals was contrasted with that of the pure form, and the doped version exhibited greater efficiency, particularly for high-frequency applications.

Keywords: **HOMO and LUMO, methyl orange, nonlinear optical studies, thermodynamic parameters, thiourea barium chloride crystal.**

Classification numbers: **2.1, 2.3**

1. Introduction

TBC is a crystal that has been extensively researched and is frequently used as a frequency doubler in laser applications. The performance of this crystal-based technology, as well as the quality of TBC crystals, can be enhanced with appropriate dopants. Dye was doped into TBC crystals to investigate the effects of dye-based dopants on the NLO properties of TBC crystals. The influence of impurity atoms on crystal quality and performance was explored. Solution growth was employed to produce bulk crystals of dye-doped TBC [1-3].

In recent decades, various NLO materials with strong non-linear susceptibilities have been identified as potential candidates for frequency conversion. Nonetheless, in actual device applications, they often exhibit inadequate transparency, poor optical quality, a lack of resilience, a low laser damage threshold, and challenges in cultivating organic materials [4-6]. Additionally, whilst the mechanical and thermal properties of large single crystals are exceptional, their non-linearity is relatively low. Hence, substantial research has been undertaken on semi-organic materials, which amalgamate the attributes of both organic and inorganic compounds [7].

Given that the majority of organic molecules are constituted by weak van der Waals and hydrogen bonds with conjugated electrons, organic materials tend to possess high SHG efficiency but are less stable. Conversely, inorganic compounds are notably stable but manifest a diminished SHG efficiency. This piques interest in semi-organic compounds, which represent a nexus between stability and efficiency. Thiourea is a compelling compound that possesses centrosymmetry but becomes non-centrosymmetric when coordinated with metal complexes [8-10].

The linear and non-linear behaviours in organic and semi-organic crystals largely hinge on their chemical properties. The chemical reactivity, stability, chemical hardness, electrophilicity index, and donor-acceptor interactions through NBO analysis in strontium chloride, palladium chloride, antimony triborate, and zinc selenate with thiourea have been extensively probed [11-14].

Numerous researchers have endeavoured to cultivate both organic and inorganic crystalline materials, which were then subjected to various analyses for catalytic, sensory purposes, pharmaceutical applications, and COVID-19 virus detection, among other biomedical applications. Novel fused triazine, thiourea derivatives, bis-thiazoles, and certain hydroxyquinolines with their metal complexes were produced and studied using various experimental and theoretical methods. Density functional theory (DFT) was employed, using the 6-311G** and LANL2DZ basis set for selected atoms. Furthermore, NBO, energy gap using HOMO and LUMO, first-order hyperpolarizability, and anisotropic polarizability were assessed for optical applications [15-18].

[*]Corresponding author: Email: prof.s.nithiyanantham@tvkgac.co.in

CC BY NC ND
Crossref Similarity Check Powered by iThenticate

In the current work, the analysis of TBC crystals, encompassing various thermodynamic and related parameters, is discussed in relation to their energies, bonding, and other models.

2. Materials and methods

All Analar grade chemicals are purchased from S.D Fine Chemicals, Mumbai, India. The purity of the chemical is 99.5% and they are used directly without further purification. The simplest and convenient method to grow crystals is adopting the Slow evaporation technique. The good quality crystals free from strain and dislocation from an aqueous solution and slow chilling (0.5°C/day) were used to generate pure TBC crystals. For Sudan doped TBC crystals, the same process is used (0.1 mol percent of Sudan dye). The solubility of the doped TBC in the solvent was determined for each dopant, and Sudan was found to have a solubility of 16 g/100 ml at 410°C. Here, the substances do not react with each other while growing. For growth tests, seed crystals with the correct shape and no macro flaws were employed. In order to maintain the temperature, the Constant Temperature Bath (CTB) was used to generate large single crystals of TBC and Sudan doped TBC with an accuracy of 0.10°C. The initial pH value, 4.5 for Sudan dye, was saturated in the mother solution. The growth was carried out for more than 18 days at a temperature of 40°C in the bath. Throughout whole experiment double distilled water can be used [19].

3. Results and discussion

3.1. HOMO-LUMO analysis

An enhancement in the gap between the bonding and anti-bonding orbitals in the molecule under study results in hypsochromic shifts. The energy disparity between the highest and lowest occupied molecular orbitals is pivotal in ascertaining the molecular electronic transport properties, as it offers an insight into electron conductivity. Based on the wave function analysis, the transition associated with the initial state of excitation, or electron absorption, is predominantly characterised by one-electron excitation from HOMO to LUMO. The energy difference between the HOMO and LUMO, indicative of electron-donating and electron-accepting capacities respectively, conveys molecular chemical stability. The other attributes of molecules are largely governed by the energy gap between the ground state and the first excited state. The frontier electron density utilises this to pinpoint the most reactive location in p-electron systems and to elucidate various reactions in conjugated systems.

Table 1. Calculated molecular properties of MOD TBC from orbital energies.

Parameter	Value (a.u.)
HOMO	-0.201642
LUMO	-0.087242
Energy gap	0.1144
SCF energy	-538.6770
η	-0.0572
μ	0.144442
χ	-0.144442
S	-17.482517
ω	-0.182373

Table 1 presents the HOMO and LUMO energies of TBC determined at the DFT level. Fig. 1 illustrates several frontier orbitals of the title compound, accompanied by their respective energies [20]. Both HOMO and LUMO in TBC are predominantly derived from the p orbital of all the compound's atoms. As depicted in Fig. 1, the HOMO is characterised by a charge distribution across the entire structure, whereas the LUMO has a charge distribution on certain carbons of the ring. For TBC (Fig. 1), the HOMO possesses a nonbonding character for some ring atoms and two oxygen atoms, whilst the LUMO displays an anti-bonding character for some pairs, including two oxygen atoms. Red and green denote positive and negative phases, respectively. The HOMO has a calculated energy of -0.201642 a.u., whereas the LUMO's calculated energy stands at -0.087242 a.u.

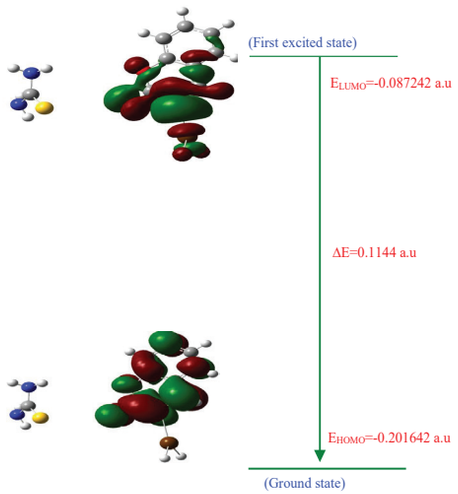

Fig. 1. The frontier molecular orbitals for MOD TBC.

Consequently, the reduction in the HOMO-LUMO band gap primarily stems from the notable stability of the LUMO due to the strong electron-accepting capacity of the electron-acceptor group. The chemical hardness (η) and chemical potential (μ) have been derived using HOMO and LUMO energies. Chemical hardness, a reactivity index, is calculated using the formula:

$$\eta = (I - H)/2 \quad (1)$$

The chemical potential, which assesses the tendency of electron clouds to escape, is given by

$$\mu = -(I + H)/2 \quad (2)$$

In a molecular system, I and H denote ionisation potential and electron affinities respectively. The inverse of hardness alludes to the flexibility of the bonding [21]. Table 1 displays the computed values of chemical properties. Recent studies have highlighted the significance of these values in ascertaining the toxicity of diverse contaminants.

3.2. Natural bond orbital analysis

The grown crystals were subjected to NBO analysis to gain insights into bond bending, rehybridisation, intramolecular charge transfer (ICT), and electron density delocalisation within the molecule. NBO calculations were conducted at the HF/6-

311++G(d,p) level using the NBO 5.0 programme, as incorporated in the Gaussian 09 package. This was done to comprehend different second-order interactions between the occupied orbitals of one subsystem and the vacant orbitals of another, reflecting delocalisation or hyperconjugation [22]. The hyperconjugative interaction energy was deduced using the second-order perturbation method:

$$E^{(2)} = \Delta E_{ij} = q_i \frac{F(i,j)^2}{\varepsilon_j - \varepsilon_i} \quad (3)$$

where $E^{(2)}$ and E_{ij} are the populations of the donor orbital, are the energies of ε_j and ε_i NBO'S, and /F/>2 or $F(i,j)^2$ is the Fock matrix element between i and j NBO orbitals. Examination of the Fock matrix in the NBO basis through second-order perturbation theory uncovers significant intermolecular hyperconjugative interactions of π-electrons, as detailed in Table 2.

Table 2. Fock matrix in NBO basis corresponding to the intramolecular bonds of MOD TBC (second order).

Donor(i)	ED(i)(e)	Acceptor(j)	ED(j)(e)	[a]E(2) (KJ/mol)	[b]E(j)-E(i)(au)	[c]F(i,j)(a.u.)
σ (C1-C2)	1.97406	σ* (C1-C6)	0.02283	3.82	1.27	0.062
σ (C1-C2)	1.97406	σ* (C2-C3)	0.01618	3.32	1.26	0.058
σ (C1-C6)	1.96974	σ* (C5-O19)	0.03239	4.31	0.97	0.058
π (C1-C6)	1.67968	π* (C2-C3)	0.37156	20.29	0.27	0.067
π (C1-C6)	1.67968	π* (C4-C5)	0.42853	22.96	0.26	0.071
σ (C2-C3)	1.97178	π* (C1-C2)	0.02340	3.63	1.27	0.061
σ (C2-C3)	1.97178	σ*(C1-C7)	0.02441	6.87	1.08	0.058
σ (C2-C3)	1.97178	σ*(C4-O17)	0.02939	4.49	0.94	0.058
π (C2-C3)	1.70600	π* (C1-C6)	0.35696	20.83	0.29	0.071
π (C2-C3)	1.70600	π* (C4-C5)	0.42853	19.87	0.27	0.068
σ (C2-H15)	1.97795	σ*(C1-C6)	0.02283	4.89	1.09	0.065
σ (C4-C5)	1.97578	σ*(C3-C4)	0.02345	4.44	1.28	0.067
π (C4-C5)	1.65314	π* (C1-C6)	0.35696	17.48	0.31	0.066
π (C4-C5)	1.65314	π* (C2-C3)	0.37156	20.85	0.30	0.071
σ (C5-C6)	1.96939	σ*(C1-C6)	0.02283	3.87	1.28	0.063
σ (C5-C6)	1.96939	σ*(C1-C7)	0.02441	3.58	1.09	0.056
σ (C5-C6)	1.96939	σ*(C4-C5)	0.03487	4.63	1.24	0.068
σ (C5-C6)	1.96939	σ*(C4-O17)	0.02939	4.38	0.95	0.058
σ (C6-H24)	1.97065	σ*(C41C2)	0.02340	4.60	1.09	0.063
σ (C6-H24)	1.97065	σ*(C4-C5)	0.03487	4.38	1.05	0.061
π (C10-H12)	1.98037	π* (C7-H9)	0.01806	3.69	0.67	0.044
σ (O17-H18)	1.99047	σ*(C4-C5)	0.03487	3.78	1.29	0.063
σ (O19-C20)	1.99209	σ*(C5-C6)	0.02109	3.38	1.35	0.061
σ (C20-H23)	1.98953	σ*(C5-O19)	0.03239	3.94	0.78	0.050
LP2(O19)	1.86933	π* (C4-C5)	0.42853	19.61	0.34	0.080
LP2(O19)	1.86933	σ*(C20-H21)	0.01652	4.93	0.72	0.055
LP2(O19)	1.86933	σ*(C20-H22)	0.01650	4.93	0.72	0.055

Owing to the pronounced interaction between the lone pair O19 and the antibonding C20-H22, the stabilisation energy of 4.93 kJ/mol indicates heightened delocalisation. Noteworthy interactions between LP2O19 and antibonding C4-C5, C20-H21 in the title molecule yield stabilisation values of 19.61 and 4.93 kJ/mol, respectively. Such interactions around the ring might augment the molecule's bioactivity. The π*(C4-C5), π*(C2-C3), and π*(C1-C6) bond orbitals facilitate an intra-molecular interaction culminating in significant intra-molecular charge transfers with stabilisation values of 227 and 145 kJ/mol, respectively. Such charge transfers can render the molecule highly nonlinear.

The second-order perturbation theory delineates various electron donor orbitals, acceptor orbitals, and the corresponding stabilisation energy. The more intense the interaction between electron donors and electron acceptors, or the higher the proclivity of donors to bequeath to acceptors, the elevated the E(2) value becomes, indicating an increased degree of conjugation within the system. A stabilising donor-acceptor interaction is manifested when electron density delocalises between occupied Lewis-type (bond or lone pair) and formally vacant non-Lewis NBO orbitals.

Intramolecular hyperconjugative interactions emerge from the orbital overlap of the (C-C) and π*(C-C) bond orbitals, facilitating ICT and system stabilisation. As a consequence of these interactions, which augment the electron density (ED) in the C-C antibonding orbital, the bonds become attenuated [23]. A pronounced intramolecular hyperconjugative interaction transfers electrons from the C1-C2, C2-C3, and C4-C5 bonds to the benzene ring's π*(C1-C6) bond, enhancing and stabilising the electron density at 50 kJ/mol.

3.3. Thermodynamic properties

A range of thermodynamic properties are delineated in Table 3. For precise prediction of the zero-point vibrational energies (ZPVE), rotational constants, thermal energy, and entropy, scaling factors have been proposed.

Table 3. Theoretically computed parameters-I.

Parameter	Value	
	LSDA	*HF*
Zero-point vibrational energy (kcal/mol)	121.44639	132.94025
Rotational constant (GHz)		
A	1.67529	1.67633
B	0.56727	0.54977
C	0.43809	0.43691

The total energy appears to diminish as the basis set dimension grows. The total capacity and entropy of the title chemical at ambient temperature exhibit minor variations across different basis sets [24] (Table 4).

Table 4. Theoretically computed parameters-II.

Parameter	Thermal energy (kcal/mol)		Entropy (cal/ mol)		Enthalpy (cal/mol·K)	
Total	129.082	140.180	109.196	107.822	45.588	41.838
Translational	0.889	0.889	41.194	41.194	2.981	2.981
Rotational	0.889	0.889	31.024	31.057	2.981	2.981
Vibrational	127.304	138.403	36.978	35.570	39.626	35.877

Table 5 catalogues the constant pressure values for heat capacities (C_p), entropies (S), and enthalpy changes ($\Delta H_{0\rightarrow T}$) for zero (monomer) and applied electric fields. These metrics derive from vibrational analysis at the HF/6-311++G(d,p) level and statistical thermodynamics. As molecular vibration intensities amplify, conventional thermodynamic functions escalate with temperature, with entropy increasing whilst enthalpy and heat capacity remain stable, as demonstrated in Table 5.

Table 5. MOD TBC determined by DFT/HF/6-311++G(d,p) method (temperature-dependent parameters).

T(K)	S ($J \cdot mol^{-1}K^{-1}$)	C_p ($J \cdot mol^{-1}K^{-1}$)	$\Delta H_{0\rightarrow T}$ ($kJmol^{-1}$)
100	379.02	30.1	8.52
200	490.88	199.95	25.05
298.15	583.95	272.06	48.6
300	585.68	273.46	48.67
400	674.66	348.35	79.79
500	759.78	415.29	118.06
600	840.61	471.26	162.48
700	916.83	517.27	211.98
800	988.45	555.24	265.67
900	1055.73	586.85	322.82
1000	1118.98	613.39	382.87

Compression at constant temperature results in a molecule's volume reduction [25-27]. The potential positions a molecule's particles can occupy become restricted with a decrease in molecular volume. Consequently, at a constant temperature, entropy tends to diminish as pressure ascends. Fig. 2 portrays the correlation graph for zero applied EFs. The fitting equations are:

$$S^0_m = 311.40643 + 1.13227T - 3.22688 \times 10^{-4}\ T^2\ (R^2=0.99981) \quad (4)$$

$$C^0_{p,m} = 6.48149 + 5.36266T - 0.0397 \times 10^{-4}\ T^2\ (R^2=0.99866) \quad (5)$$

$$H^0_m = -5.87053 + 2.49217T - 0.0397 \times 10^{-4}\ T^2\ (R^2=0.99960) \quad (6)$$

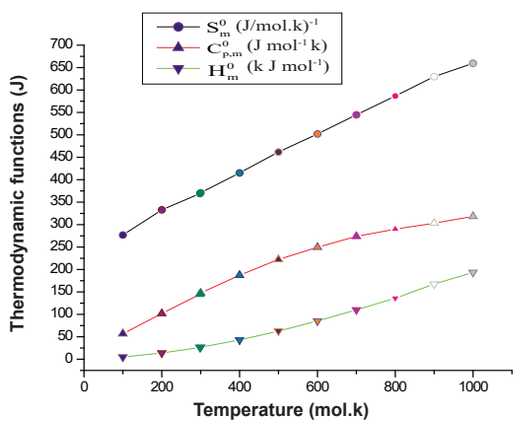

Fig. 2. Correlation of MOD TBC at various temperatures.

3.4. Electrostatic potentials

Constructing a three-dimensional ESP map over molecular surfaces using experimental charge densities markedly accentuates the electrostatic character of the three configurations (Figs. 3-5).

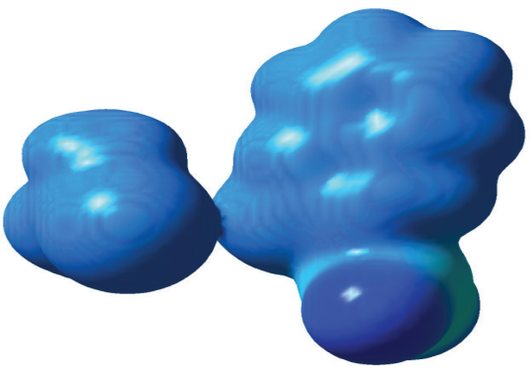

Fig. 3. MOD TBC (electron density).

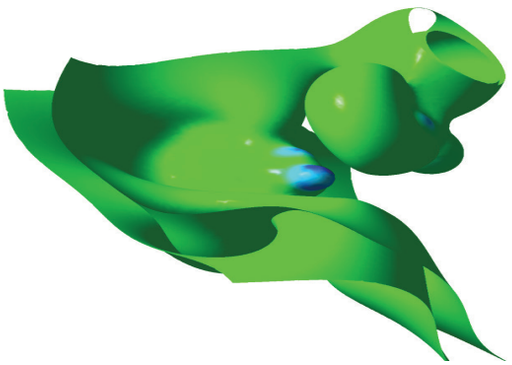

Fig. 4. Electrostatic potential surface of MOD TBC (contour map).

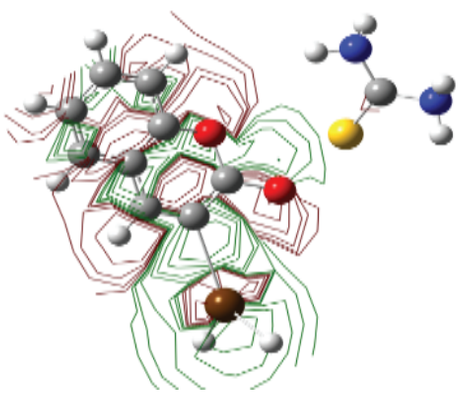

Fig. 5. Electron density maps of MOD TBC.

The electropositive and electronegative surfaces are clearly differentiated in Fig. 4. ESP mapping reveals a broader electronegative surface, attributed to the conformational difference of the C-O side chain, the involvement of electrons of the triad C1-C2-H12 in C-H... type interactions, and the presence of π, π... contacts.

The electronegative surface predominantly surrounds oxygen atoms in C-H...O type intermolecular interactions. However, in contrast to other Ba atoms in the structures, atom O11 exhibits a less pronounced electronegative surface. This stems from atom O11's lack of engagement in intermolecular interactions, whilst a comparable atom in S is seen to interact with the neighbouring molecule (Fig. 5). The theoretical analyses' affiliated maps display analogous traits. The ESP maps lucidly highlight the optimal binding sites to construct interaction networks and the variances in interaction modalities [28].

3.5. NLO studies

The crystallinity of MOD TBC, pertaining to its suitability for NLO applications, and its frequency, were examined employing a solid-state laser [29] (Table 6).

Table 6. NLO efficiency of TBC.

No.	Compound	NLO efficiency
1	Pure TBC crystals	1.79
2	MOD TBC crystals	1.89

Determined using the S.K. Kurtz, et al.'s powder method (1968) [30], the crystal was placed and the optical beam input realigned. Its significance was subsequently analysed in conjunction with green light. Comparing the NLO efficiency of the doped crystal to pure TBC reveals that the former boasts superior efficiency and broader applications [31-34]. Both TBC variants, including the doped version, underwent NLO measurement. The NLO efficiencies of pure TBC and MOD TBC crystals are presented in Table 6.

4. Conclusions

Single crystals of pure and dye-doped TBC with well-defined optical quality were synthesised through slow solvent evaporation. Furthermore, optically superior quality crystals of TBC with enhanced dye-doped TBC have been examined. The inherent electronic parameters affiliated with the orbitals manifest in the notable electronic energy gaps of molecules. These orbitals not only delineate how a molecule interacts within its species but also juxtapose the efficacy of the doped TBC against its pure crystalline counterpart. The correlation in thermal properties leans favourably towards the dopant rather than the pure crystal. A heightened electronegativity is discernible in the doped crystal. The doped crystal was observed to amplify the NLO attribute of TBC crystals. The MOD TBC crystal demonstrated 1.89 times the SHG performance of KDP and 1.05 times that of pure TBC crystal. The electron distribution in metallic elements significantly influences the chemical bond.

CRediT author statement

S. Panimalar: Conceptualisation, Methodology, Formal analysis; P. Kumaresan, K.S. Kumar, R. Mohan: Software, Data curation, Validation, Visualisation, Investigation; S. Nithiyanantham: Conceptualisation, Methodology, Formal analysis, Supervision, Writing original draft preparation, Writing - Review and Editing, Project administration.

COMPETING INTERESTS

The authors declare that there is no conflict of interest regarding the publication of this article

REFERENCES

[1] P. Girija, S. Parthiban, S.C. Mojumdar (2015), "Influence of picric acid on SHG efficiency of tris (thiourea) zinc(II) sulphate (ZTS)", *Journal of Thermal Analysis and Calorimetry*, **119**, pp.953-958, DOI: 10.1007/s10973-014-4238-9.

[2] S.E.A. Moses, S. Tamilselvan, S.M.R. Kumar, et al. (2019), "Synthesis, growth and characterization of semi-organic nonlinear optical L-threnoninum sodium fluoride (LTSF) crystal for photonics application", *Chinese Journal of Physics*, **58**, pp.294-302, DOI: 10.1016/j.cjph.2019.01.016.

[3] M.S.H. Faizi, F.A.P. Osório, C. Valverde (2020), "Synthesis, crystal structure, spectroscopic and nonlinear optical properties of organic salt: A combined experimental and theoretical study", *Journal of Molecular Structure*, **1210**, DOI: 10.1016/j.molstruc.2020.128039.

[4] A. Subashini, K. Rajarajan, S. Sagadevan (2017), "Synthesis, growth, spectral, optical and thermal studies of thiourea family crystal: TTPB", *Material Research Express*, **4(2)**, DOI: 10.1088/2053-1591/aa5d94.

[5] B. Jalel, N. Ennaceur, S. Hawech, et al. (2019), "Synthesis and characterization of a metal-organic NLO material: Tetrakis (thiourea) cobalt chloride", *Journal of Physics and Chemistry of Solids*, **133**, pp.35-45, DOI: 10.1016/j.jpcs.2019.04.036.

[6] Y. Yang, Z. He, J. He, et al. (2020), "The influence on properties with different nonlinear optical materials", *Dyes and Pigments*, **176**, DOI: 10.1016/j.dyepig.2020.108219.

[7] K. Mahendra, A. D'Souza, N.K. Udayashankar (2017), "Synthesis, structural, optical and electrical (DC) properties of a semiorganic thiourea barium chloride (TBC) single crystal", *Optik*, **145**, pp.436-447, DOI: 10.1016/j.ijleo.2017.07.054.

[8] N. Sivakumar, V. Jaisankar, G. Chakkaravarthi, et al. (2014), "Synthesis, crystal structure, optical, thermal and mechanical characterization of poly bis(thiourea) silver(I) nitrate single crystals synthesized at room temperature", *Materials Letters*, **132**, pp.298-301, DOI: 10.1016/j.matlet.2014.06.079.

[9] S. Shanmugan, N. Saravanan, V. Chithambaram, et al. (2020), "Investigation on single crystal by tartaric acid-barium chloride: Growth and characterization of novel NLO materials", *Bulletin of Materials Science*, **43**, DOI: 10.1007/s12034-020-02176-6.

[10] C.R.T. Kumari, A. Al Otaibi, T. Kamaraj, et al. (2021), "A brief study on optical and mechanical properties of an organic material: Urea glutaric acid (2/1) - A third order nonlinear optical single crystal", *Crystals*, **11(10)**, pp.2073-4352, DOI: 10.3390/cryst11101239.

[11] N.R. Rajagopalan, P. Krishnamoorthy, K. Jayamoorthy, et al. (2016), "Bis (thiourea) strontium chloride as promising NLO material: An experimental and theoretical study", *Karbala International Journal of Modern Science*, **2(4)**, pp.219-225, DOI: 10.1016/j.kijoms.2016.08.001.

[12] N.R. Rajagopalan, P. Krishnamoorthy, K. Jayamoorthy, et al. (2017a), "Synthesis, characterization, nucleation kinetics, mechanical, photo conductivity, birefringence and DFT studies of tris (thiourea) zinc selenate as potential NLO material", *J. Inorg. Organomet. Polym.*, **27**, pp.1199-1210. DOI: 10.1007/s10904-017-0567-z.

[13] N.R. Rajagopalan, P. Krishnamoorthy, K. Jayamoorthy (2018), "Experimental and theoretical investigations of tetrakis (thiourea) palladium chloride semi-organic non-linear optical crystal: An approach to NLO application", *Silicon*, **10**, pp.841-850, DOI: 10.1007/s12633-016-9538-1.

[14] N.R. Rajagopalan, P. Krishnamoorthy, K. Jayamoorthy (2017b), "Synthesis, characterization, thermal analysis, nucleation kinetics and DFT studies of Bis(thiourea) antimony tribromide as potential NLO material: Comparison of experimental and computational studies", *J. Inorg. Organomet. Polym.*, **27**, pp.1457-1465, DOI: 10.1007/s10904-017-0602-0.

[15] A.M. Ibrahim, F.M. Abdel-Haleem, A. Salah, et al. (2022), "Development of potentiometric sensors based on thiourea derivatives, Gd_2O_3@rGO and MoO_3@rGO for the determination of salicylate in drug tablets and biofluids and DFT studies", *Microchemical Journal*, **183**, DOI: 10.1016/j.microc.2022.108064.

[16] A.H.M. Elwahy, E.M. Eid, S.A. Abdel-Latif, et al. (2023), "Design, synthesis, DFT, TD-DFT/PCM calculations, and molecular docking studies on the anti-COVID-19, and Anti-SARS activities of some new bis-thiazoles and bis-thiadiazole", *Polycyclic Aromatic Compounds*, **43(7)**, pp.6407-6436, DOI: 10.1080/10406638.2022.2117204.

[17] H.A.S. Al-Shamiri, M.E.M. Sakr, S.A. Abdel-Latif, et al. (2022), "Experimental and theoretical studies of linear and non-linear optical properties of novel fused-triazine derivatives for advanced technological applications", *Sci. Rep.*, **12**, DOI: 10.1038/s41598-022-22311-z.

[18] M.G. Abd El-Nasser, S.A. Abdel-Latif (2023), "Ligational behavior of bidentate nitrogen-oxygen donor 8-quinolinolazodye toward Ni^{2+} and Zn^{2+} ions: Preparation, spectral, thermal, experimental, theoretical, and docking studies", *Applied Organometallic Chemistry*, **37(3)**, DOI: 10.1002/aoc.6998.

[19] A. Mermer, H. Bayrak, S. Alyar, et al. (2020), "Synthesis, DFT calculations, biological investigation, molecular docking studies of β-lactam derivatives", *Journal of Molecular Structure*, **1208**, DOI: 0.1016/j.molstruc.2020.127891.

[20] T. Kubendiran, S.M.R. Kumar, S.E.A. Moses, et al. (2019), "Second and third order nonlinear optical, mechanical, surface characteristics of bis(thiourea) manganese chloride (BTMC) grown by slow cooling technique used for frequency conversion applications", *Journal of Materials Science: Materials in Electronics.*, **30**, pp.17559-17571, DOI: 10.1007/s10854-019-02105-2.

[21] C.D.D. Mveme, F.T. Nya, G.W. Ejuh, et al. (2020), "Density functional theory study of optoelectronic, nonlinear optical, piezoelectric and thermodynamic properties of poly (3,4-ethylenedioxythiophene), poly(3,4-ethylenedioxyselenophene) and their derivatives", *Optical and Quantum Electronics*, **52**, DOI: 10.1007/s11082-020-02492-5.

[22] B. Latha, P. Kumaresan, S. Nithiyanantham, et al. (2017), "Spectroscopic, HOMO-LUMO and NLO studies of tetra fluoro phthalate doped coumarin crystals using DFT method", *Journal of Molecular Structure*, **1142**, pp.255-260, DOI: 10.1016/j.molstruc.2017.04.078.

[23] B. Chandralekha, R. Hemamalini, S. Muthu, et al. (2020), "Spectroscopic (FT-IR, FT-RAMAN, NMR, UV-Vis) investigations, computational analysis and molecular docking study of 5-bromo-2-hydroxy pyrimidine", *Journal of Molecular Structure*, **1218**, DOI: /10.1016/j.molstruc.2020.128494.

[24] H. Arı, T. Ozpozan, Y. Kabacalı, et al. (2020), "Monomeric or dimeric? A theoretical and vibrational spectroscopic approach to the structural stability of 5-(4-metoxy benzoyl)-6-(4-metoxyphenyl)-3-methyl-2-thioxo-2,3-dihydropyrimidine-4(1H)-on", *Journal of Molecular Structure*, **1222**, DOI: 10.1016/j.molstruc.2020.128848.

[25] D.C.M. Glory, K. Sambathkumar, R. Madivanane, et al. (2017), "Enhancement of atom transfer in different surface chemistry of hydrogenated vs. fluorinated tribromobenzene on Ag(111) and Cu(111)", *Journal of Molecular Structure*, **1149**, pp.112-127, DOI: 10.1016/j.molstruc.2017.07.073.

[26] V. Vidhya, A. Austine, M. Arivazhagan (2020), "Experimental approach, theoretical investigation and molecular docking of 2-chloro-5-fluoro phenol antibacterial compound", *Heliyon*, **6(11)**, DOI: 10.1016/j.heliyon.2020.e05464.

[27] C. Raveendiran, P. Prabukanthan (2021), "Synthesis, crystal growth, crystal arrangement, optical, thermal, NLO and biological investigations of heterocyclic compounds of N-(1,3-benzothiazol-2-yl)benzamide and N-(1,3-benzothiazol-2-yl)-2-fluorobenzamide", *European Jour. Eng. Tech. Res.*, **6(5)**, pp.181-189, DOI: https://doi.org/10.24018/ejers.2021.6.5.2554.

[28] S. Vasumathi, H.J. Johnson, P. Selvarajan (2021), "Spectral, NLO, thermal, hardness and SEM studies of phosphate doped bis-urea oxalic acid crystals for laser applications", *Chinese Journal of Physics*, **73**, pp.1-12, DOI: 10.1016/j.cjph.2021.06.008.

[29] K. Sambathkumar, S. Nithiyanantham (2017), "Synthesis, characterization and theoretical properties of coumarin NLO single crystal by DFT method", *Journal of Material Science: Materials and Electronics*, **28**, pp.6529-6543, DOI: 10.1007/s10854-017-6342-7.

[30] S.K. Kurtz, T.T. Perry (1968), "A powder technique for the evaluation of nonlinear optical materials", *J. Appl. Phys.*, **39**, pp.3798-3813, DOI: 10.1063/1.1656857.

[31] K. Mahendra, A.D. Souza, Ifthekarahmed, et al. (2018), "Synthesis and optical characterization of amaranth dye doped thiourea barium chloride (TBC) single crystals", *Materials Today Proceeding*, **5**, pp.16358-16366, DOI: 10.1016/j.matpr.2018.05.132.

[32] D.C.M. Glory, K. Sambathkumar, R. Madivanane, et al. (2018), "Optical, fluorescence with quantum analysis of hydrazine (1, 3-dinitro phenyl) by DFT and Ab initio approach", *Journal of Molecular Structure*, **1163**, pp.480-495, DOI: 10.1016/j.molstruc.2017.12.046.

[33] A. Anbarasi, S.M.R. Kumar, M.P. Raj, et al. (2019), "Synthesis, growth and characterization of semiorganic nonlinear optical single crystal bis(thiourea) barium nitrate (BTBN) for frequency conversion", *Materials Science-Poland*, **37(3)**, pp.381-388, DOI: 10.2478/msp-2019-0039.

[34] V. Chithambaram, T.S.F. Rajesh, G. Palani, et al. (2020), "Growth and investigation of novel nonlinear optical single crystal of urea potassium dichromate by solution growth technique for photonic application", *Journal of Optics*, **49**, pp.181-186, DOI: 10.1007/s12596-020-00605-7.